Transport in Porous Media **26:** 277–297, 1997.

Micromodel Observation of the Role of Oil Layers in Three-Phase Flow

ARTURO A. KELLER[1], MARTIN J. BLUNT[2] and PAUL V. ROBERTS[3]
[1]*School of Environmental Science and Management, University of California, Santa Barbara, CA 93106-5131. e-mail: keller@esm.ucsb.edu*
[2]*Petroleum Engineering Department, Stanford University, Stanford, CA 94305. e-mail: blunt@pangea.stanford.edu*
[3]*Environmental Science and Engineering Program, Civil Engineering Department, Stanford University, Stanford, CA 94305-4020. e-mail: pvr@cive.stanford.edu*

(Received: 22 February 1996; in final form: 24 September 1996)

Abstract. We have studied the flow of a non-aqueous phase liquid (NAPL, or oil), water and air at the pore scale using a micromodel. The pore space pattern from a photomicrograph of a two-dimensional section through a Berea sandstone was etched onto a silicon wafer. The sizes of the pores in the micromodel are in the range 3–30 μm and are the same as observed in the rock from which the image was taken. We conducted three-phase displacement experiments at low capillary numbers (in the order of 10^{-7}) to observe the presence of predicted displacement mechanisms at the pore scale. We observed stable oil layers between the wetting phase (water) and the non-wetting phase (gas) for the water–decane–air system, which has a negative equilibrium spreading coefficient, as well as four different types of double displacements where one fluid displaces another that displaces a third. Double imbibition and double drainage are readily observed, but the existence of an oil layer surrounding the gas phase makes the other double displacement combinations very unlikely.

Key words: NAPL, multiphase flow, three-phase flow, film flow, micromodel, spreading coefficient, non-spreading oil.

1. Introduction

Understanding two- and three-phase flow in porous media is important in many engineering fields, for example in environmental modeling of flow of a nonaqueous phase liquid (NAPL) in the subsurface, the recovery of oil from underground reservoirs in the presence of gas and water phases, and chemical engineering applications. Two-phase flow is reasonably well understood and can be adequately modeled at the macroscopic level using the concepts of relative permeabilities and capillary pressures as a function of saturation. Two-phase studies at the pore scale level, both experimental (e.g. Mohanty *et al.*, 1994; Vizika *et al.*, 1994; Billiote *et al.*, 1993; Lenormand and Zarcone, 1988; Lenormand *et al.*, 1983) and with network models (e.g. Berkowitz and Balberg, 1993; Sahimi, 1993; Blunt *et al.*, 1992; Blunt and King, 1991; Lenormand and Zarcone, 1987; Touboul *et al.*, 1987; Dias and Payatakes, 1986) provide a physical framework for the functional relationships between relative permeability or capillary pressure and saturation.

The effect of heterogeneities (Ferrand and Celia, 1992; Jerauld and Salter, 1990), flow in fractured media with a porous matrix, surfactants, miscible fluids and wetting properties of porous media (McDougall and Sorbie, 1995) are some of the remaining challenges in two-phase flow.

The multiphase flow behavior is complicated by the introduction of a third fluid phase into the porous medium. This may occur as a result of the natural movement of the water table, when oil is either trapped in ganglia above or below the water table or floating as a pool on top of the water table. In addition, active injection of a gaseous or aqueous phase to remove oil, for example water flooding, steam injection and gas injection in oil reservoirs or dewatering for soil vapor extraction, all result in three-phase flow conditions. Much of the early work on three-phase flow has been concentrated on developing empirical correlations for three-phase relative permeabilities and capillary pressure curves as a function of phase saturation(s) (Parker and Lenhard, 1990; Fayers, 1989; Baker, 1988; van Genuchten, 1980; Stone, 1973, 1970), based on numerical matching of limited experimental and field data. These empirical three-phase relative permeabilities do not adequately represent the physics of oil flow at low oil saturation, which is of importance for predicting NAPL saturations for environmental remediation schemes or to evaluate the efficiency of a tertiary oil recovery project.

More recently, researchers have attempted to incorporate a physical explanation for the functional form of the relative permeability and capillary pressure relationships at the pore scale level using network models (Fenwick and Blunt, 1996; Oren *et al.*, 1994; Soll and Celia, 1993) and micromodel studies (Dong *et al.*, 1995; Oren and Pinczewski, 1995; Soll *et al.*, 1993; Oren *et al.*, 1992; Chatzis *et al.*, 1988). The micromodel studies by Oren and Pinczewski (1995), Soll *et al.* (1993) and Oren *et al.* (1992) were conducted on regular networks with pore spaces at least ten times larger than those seen in most consolidated or unconsolidated porous media, which leads to relatively large capillary numbers. Our study involves irregular networks with pores ranging in size from 3 to 30 μm across, and flow at low capillary numbers. These conditions are representative of those observed for natural displacements.

We consider water to be the most-wetting phase on the clean solid surface. The gas phase is the most nonwetting phase. The oil phase is usually of intermediate wettability. Depending on the interfacial tensions of the three phases, oil may spread between water and gas, or may form a droplet. Over a flat water surface, a spreading oil will eventually form a thin film of molecular thickness, a few nanometers across at most. In a porous medium, a spreading oil will coat all water/gas interfaces with a molecular film, but the flow rates through these films are negligible and cannot account for any appreciable movement of oil (Blunt *et al.*, 1995). To be of significance for flow, oil must form a layer between water and gas in the crevices or roughness in the pore space. These layers may be on the order of one or more micrometers (Blunt *et al.*, 1995). Three-phase flow experiments in sand columns (Blunt *et al.*, 1995) indicate that very low residual NAPL saturations can be achieved

(on the order of 1 per cent) even for systems with negative spreading coefficients, which indicates that after the main NAPL front passes, additional flow must be through layers in the crevices. We distinguish between molecular films, through which there is negligible flow, and layers which may account for significant oil migration.

Although it was initially considered that only spreading oils could form layers in a porous medium, Dong *et al.* (1995) have theoretically predicted and experimentally verified that nonspreading oils can form thick layers in the crevices of the pore space, depending not only on the spreading coefficient and capillary pressures but also on the geometry of the crevice. Thick oil layers may provide additional channels for oil flow at low oil saturations, resulting in very low residual oil saturations. Because many NAPLs of environmental significance are nonspreading, the role of oil layers is important in modeling the flow of three phases in the subsurface. Blunt *et al.* (1995) observed rapid oil (iso-octane) layer flow in the corners using capillary tubes with square cross-section, in a time-frame that is environmentally significant. In micromodel studies, oil layers have been observed for Soltrol, which is spreading (Oren and Pinczewski, 1995). For nonspreading oils, Oren and Pinczewski (1995) and Oren *et al.* (1992) did not observe oil layers.

In addition to piston-like displacement of the residing phase by the invading phase, and the trapping mechanisms observed in two-phase flow (Lenormand, 1988), six additional displacement mechanisms can occur when the three phases are present in the same pore space, as discussed below. Oren and Pinczewski (1995) observed double drainage, where gas displaces oil that displaces water.

In this study, we extend our investigation of the role of oil layers in three-phase flow by observing the various displacement mechanisms in a micromodel, which contains corners that allow for oil flow in layers. Our motivation is to find if oils with negative spreading coefficients can form layers, and the significance of these layers for reaching very low oil saturations. The observations are directed to understand displacement mechanisms at the pore scale, but not to study overall displacement efficiency, which is better understood from three-dimensional laboratory experiments. The results of this study can be used in network models to study physically based relative permeabilities and capillary pressure relationships. We briefly review the theoretical background for the existence of oil layers, followed by a description of the experimental setup, and then we present our observations.

2. Theory

2.1. SPREADING COEFFICIENT

The spreading coefficient, C_S is defined as

$$C_S = \gamma_{gw} - (\gamma_{ow} + \gamma_{go}), \tag{1}$$

using the subscripts w for water, o for oil and g for gas. Typically, $\gamma_{gw} > \gamma_{ow} > \gamma_{go}$, but the magnitude of the sum of interfacial tensions $\gamma_{go} + \gamma_{ow}$ can be larger

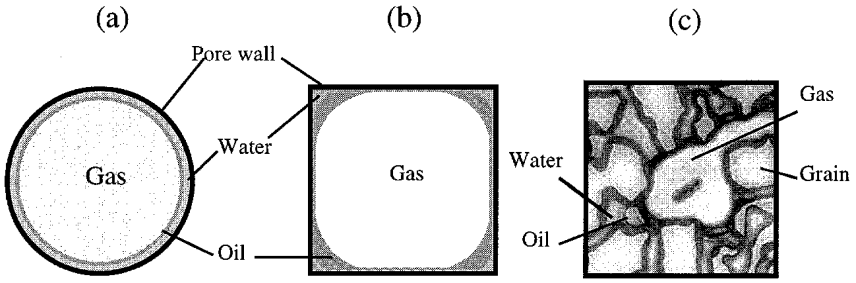

Figure 1. Three phases in a single pore space, for (a) a circular cross-section, (b) a rectangular cross-section and (c) a realistic pore space configuration.

than γ_{gw}, resulting in a negative spreading coefficient, as is the case for many hydrocarbons (e.g. decane and higher hydrocarbons) and chlorinated solvents (e.g. carbon tetrachloride, trichloroethylene, tetrachloroethylene) as well as for some oil mixtures. This means that, on a flat surface, oil will form droplets and will not spread. If $C_S > 0$, the oil will spread between water and gas, as occurs for the lighter hydrocarbons.

The interfacial tensions can change as the interfaces age, i.e. they become contaminated with molecules from the other fluids. Even for fairly immiscible fluids, the dissolution of oil in water, the volatilization of oil and water to the gas phase, and the formation of molecular oil films over the gas/water interface (if $C_S > 0$), result in a decrease in γ_{gw} that is usually larger than the changes in γ_{go} and γ_{ow} , resulting in a change in the spreading coefficient. The aged spreading coefficient is considered here as the equilibrium spreading coefficient, C_s^e. When thermodynamic equilibrium is reached, $C_s^e \leqslant 0$ (Adamson, 1990).

2.2. OIL LAYERS

Free-energy calculations and experimental work by Dong *et al.* (1995) have shown that oil layers may exist in a porous matrix for $C_s^e \leqslant 0$, and that the oil phase will imbibe into crevices in the porous medium. Fenwick and Blunt (1996) have shown theoretically that layers of oil may be present in a crevice, provided that the geometry and ratio of capillary pressures are within certain ranges. Figure 1 presents the situation for (a) a circular cross-section, (b) a square cross-section and (c) a more realistic pore space configuration. In the case of the circular cross-section, only a film will exist if $C_S > 0$, and will be very thin, of molecular thickness. Flow through these thin films is very slow, and may result in drainage of oil phase from the porous media only over very long time frames. On the other hand, these very thin films present a large surface area for volatilization of the oil to the gas phase. For the configurations in Figures 1(b) and 1(c), thick oil layers may be present.

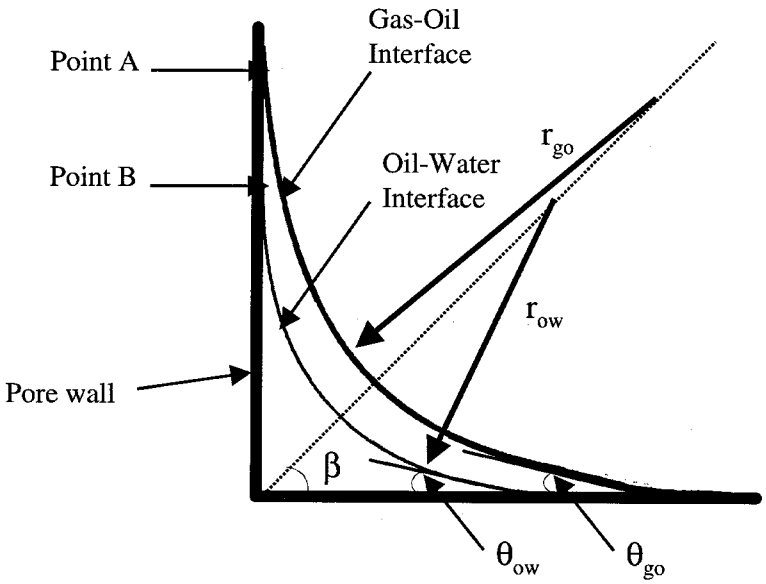

Figure 2. Geometry of a crevice with a stable oil layer between the air and water phases. The oil layer is no longer stable when the contact points A and B coincide.

For the geometry of a crevice shown in Figure 2, an oil layer will be present as long as the ratio of the oil–water interfacial radius, r_{ow}, to the gas–oil radius, r_{go}, is below a critical ratio, R_c. Fenwick and Blunt (1996) assumed that the oil layer would disappear when the oil/water and gas/oil contacts with the solid surface coincided, i.e. when points A and B in Figure 2 meet. Thus

$$\begin{aligned} R_c &= (r_{ow}/r_{go})_c = (\gamma_{ow} Pc_{go}/\gamma_{go} Pc_{ow})_c \\ &= \cos(\theta_{go} + \beta)/\cos(\theta_{ow} + \beta), \end{aligned} \tag{2}$$

where β is the half-angle of the crevice, θ_{go} is the gas/oil contact angle and θ_{ow} is the oil/water contact angle, and assuming that $\theta_{go} \geqslant \theta_{ow}$. Having three phases in equilibrium imposes a constraint on the contact angles and interfacial tensions (Zhou and Blunt, 1996)

$$\gamma_{gw} \cos\theta_{gw} = \gamma_{go} \cos\theta_{go} + \gamma_{ow} \cos\theta_{ow}, \tag{3}$$

where θ_{gw} is the gas/water contact angle measured at thermodynamic equilibrium.

For a completely water-wet surface, $\theta_{gw} = \theta_{ow} = 0$, and from Equations (1) and (2) we find (Kalaydjian, 1992)

$$\cos\theta_{go} = 1 + C_s^e/\gamma_{go}. \tag{4}$$

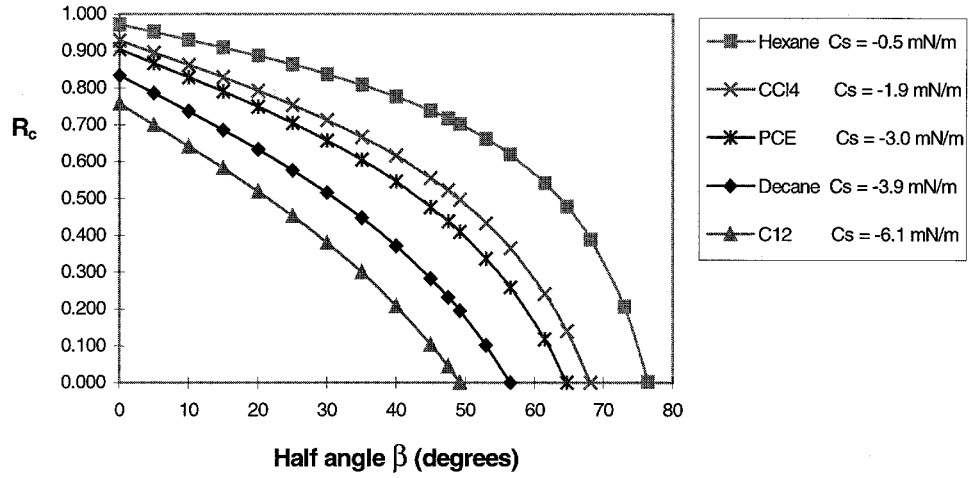

Figure 3. Dependence of critical radius, R_c, on the half angle β of the crevice and the equilibrium spreading coefficient, C_s^e. Equilibrium spreading coefficients are obtained from Hirasaki (1993).

In Figure 3 we explore the relationship between the half-angle and the critical ratio, for several nonaqueous phase liquids of environmental significance, with $C_s^e < 0$. We assume a completely water-wet medium, with $\theta_{ow} = 0$. The ratio of interfacial radii, $R = r_{ow}/r_{go}$, goes to zero as the crevice becomes wider. At $R = 0$, only oil and a water layer or gas and a water layer can occupy the crevice, but not the three phases. As R increases, all three phases can coexist in a crevice. When R_c is reached the oil layer becomes unstable and disappears. In the limit, for $\beta = 90°$, we have the configuration of a circular capillary tube, and only for a spreading oil with $C_s^e = 0$ can oil layers exist. In fact, if $C_s^e = 0$, then $R_c = 1$ for all values of β, if $\theta_{ow} = 0$. As C_s^e becomes more negative, the range of radii and crevice angles where oil layers can occur decreases.

The micromodel experiments of Oren *et al.* (1992) were performed in strongly water-wet media ($\theta_{ow} \approx 0$) with 'eye' shaped crevices for either 'spreading' systems with $C_s^e = 0$ or for oil with a large and negative spreading coefficient ($C_s^e = -8\,\mathrm{mN\,m^{-1}}$). Figure 3 indicates why oil layers were observed for the spreading fluids, but were absent for the nonspreading oils. However, many oils have a spreading coefficient that is only slightly negative ($C_s^e > -5\,\mathrm{mN\,m^{-1}}$), and the porous medium may not be completely oil-wet ($\theta_{ow} \neq 0$). For instance, in the work of Soll *et al.* (1993), $\theta_{ow} = 55°$. In this case, while the presence of oil layers does depend on the interfacial tensions, and thus indirectly on the spreading coefficient, it is evident that the assertion that spreading systems result in oil layers while nonspreading systems do not is simplistic. The point to emphasize here is that the existence of molecular films (governed by the initial value of C_s) is of negligible importance in analyzing flow in porous media – it is the presence of macroscopic

oil layers that is significant, whose existence depends on the interfacial tensions, the contact angles, C_s^e and the capillary pressures.

In our experiments with decane in pores with a rectangular cross-section, Figure 2 implies that $R_c \approx 0.28$, which means that oil layers will only be observed if the oil/water capillary pressure is much greater than the gas/oil capillary pressure. As we will show later, the ratio of curvatures in our experiments is actually much larger than R_c. However, in our micromodels, $\theta_{ow} \neq 0$. Increasing θ_{ow} aids the formation of oil layers (Equation (2)) and allows them to be stable over a much larger range of capillary pressures than for a completely water-wet medium.

2.3. DOUBLE DISPLACEMENT MECHANISMS

When the three phases are present in a region of the pore space, six possible double displacements can occur (Fenwick and Blunt, 1995), where one phase displaces another which displaces the third. The six possible double displacement combinations are shown in Figure 4 for the case where no oil layers form and the case where oil layers are stable. Double drainage (DD) and double imbibition (II) are mechanisms that may mobilize trapped oil. In addition we may observe direct two-phase displacements. These may be drainage events (gas into oil, oil into water or gas into water), or imbibition by piston-like advance or snap-off (oil into gas, water into oil and water into gas).

If oil forms a layer between gas and water, direct displacements of gas by water or vice versa are unlikely to be seen. In terms of the three-phase mechanisms shown in Figure 4, this implies that only DD and II will be observed, since the other double displacements involve gas–water contacts during an intermediate stage. As we show later, DD and II are indeed the most common double displacements. We only observe the other events when oil layers are not present, and direct gas/water displacements are possible.

This study will use a two-dimensional physical model, at low capillary numbers, to confirm (1) whether or not oil layers exist for a system with negative spreading coefficient, and (2) to observe double displacement mechanisms at the pore scale.

3. Experimental Setup

A thin slice of Berea sandstone was imaged through an optical microscope and then digitized by Hornbrook *et al.* (1991). To improve the connectivity in the two-dimensional micromodel, the digitized image was modified slightly. The pattern was then repeated 100×100 times. The digital image of the pore space was then transferred to a chrome plated glass mask, at no magnification from the original sandstone thin slice. Using technology similar to the manufacture of microchips, the image was photochemically etched on a silicon wafer, at a constant etching thickness of 15 μm. The final etched repeat pattern is shown on Figure 5. Pore diameters are in the range from 3 to 30 μm. Figure 6 is a scanning electron micrograph

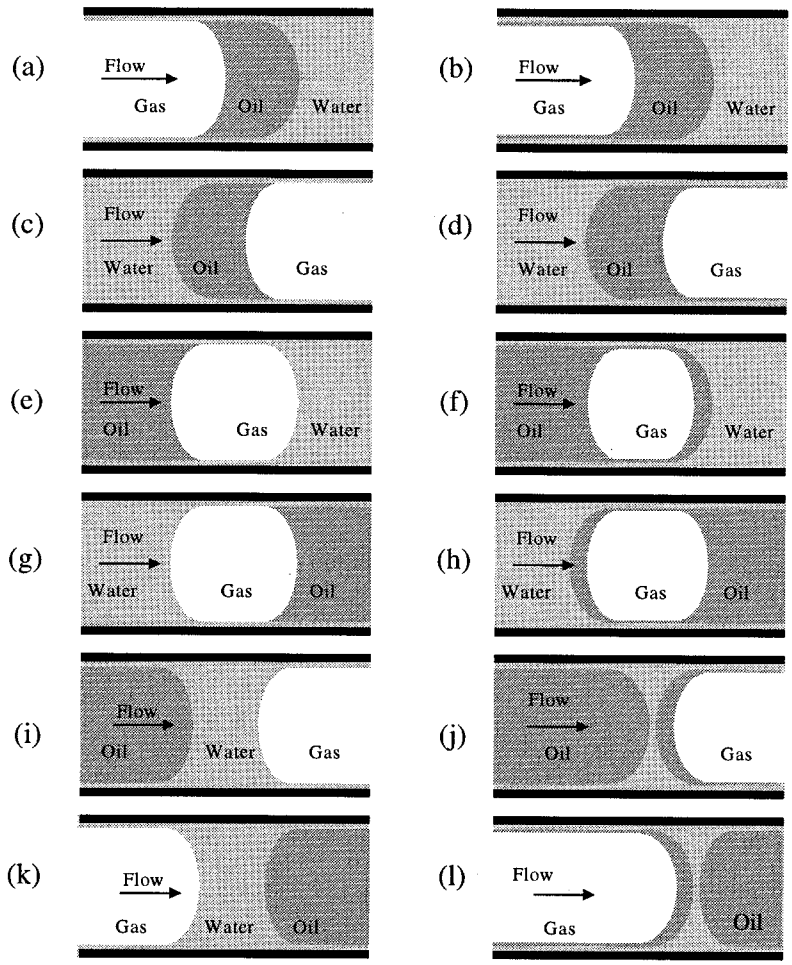

Figure 4. Possible three-phase displacements in a pore cavity: (a) DD, double drainage, where gas displaces oil that displaces water, (b) DD with an oil layer, (c) II, double imbibition, where water displaces oil that displaces gas, (d) II with an oil layer, (e) DID, imbibition–drainage with overall drainage, where oil displaces gas that displaces water, (f) DID with an oil layer, (g) IID, imbibition–drainage with overall imbibition, where water displaces gas that displaces oil, (h) IID with an oil layer, (i) IDI, drainage–imbibition with overall imbibition, where oil displaces water that displaces gas, (j) IDI with an oil layer, (k) DDI, drainage–imbibition with overall drainage, where gas displaces water that displaces oil, (l) DDI with an oil layer.

of a section of the repeat pattern, which shows the shape of the grain walls (square corners) and the regularity of the etching depth. Notice the crevices in the grain geometry. The porosity of the micromodel has been experimentally determined to be 35 per cent. We are able to make identical micromodels, for different studies.

The silicon wafer was then placed between two glass plates. The top glass plate was attached to the silicon wafer using anodic bonding. Four ports were constructed

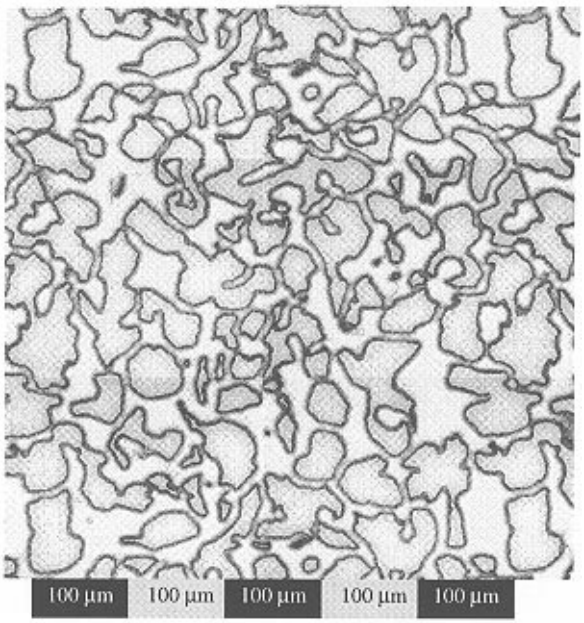

Figure 5. Composite image of the etched repeat pattern in the micromodel, which is approximately 509 × 509 μm, and etched to a depth of about 15 μm. Pore throats are on the order of 3 to 20 μm in diameter and the pores may be up to 50 μm across. The pattern is repeated 100 × 100 times in the micromodel, forming a square domain, with the inlet and outlet ports on each of the corners. A scale is shown at the bottom for reference.

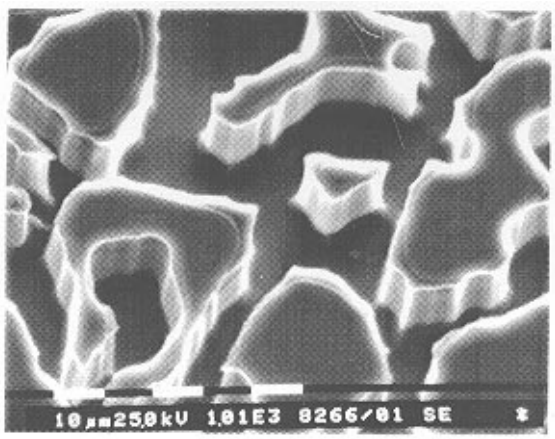

Figure 6. Scanning Electron Microscope image of the repeat pattern in the silicon wafer, without the top glass plate. The sharp edges of the 'grain' walls result in a rectangular cross-section. Oil layers may form in the square corners of the micromodel.

on the top plate to allow independent injection of three phases and an outlet port. The bottom plate was attached with epoxy, and is mainly to provide support for the micromodel. In some micromodels, a linear channel approximately 100 μm wide was etched between two ports, to have better control over the entry of an invading phase into the porous region.

Although a two-dimensional network cannot have the same connectivity as a three-dimensional network of pores, the continuity of the wetting water layer and the oil layers can still be preserved by the rectangular flow cross-section.

The silicon surface is oxidized by oxygen after etching, leaving a water-wet silica surface, approximately 10 nm deep. To ensure that the model remains water-wet, carbon dioxide is introduced to displace the air, and then water is injected, which eventually dissolves the carbon dioxide, allowing the wetting fluid to saturate the model completely. This was followed by injection of a 10 per cent acetic acid solution into the micromodel for at least 50 pore volumes. The acetic acid was flushed out with distilled water for at least 100 pore volumes, before drainage or three-phase experiments were conducted. In all cases the model is strongly water-wet ($\theta_{gw} \approx 0$) in the presence of air. Examination of oil/water interfaces indicate the model is only weakly water-wet in the presence of oil, although it is difficult to judge this accurately, since we cannot measure the vertical interfacial curvature. Water is seen to flow through crevices in oil-filled pores, which implies $\theta_{ow} < 45^\circ$. However, some oil/water interfaces appear almost perpendicular to the grain surface, indicating a contact angle significantly larger than 0°.

The experimental setup is shown in Figure 7. The light from the microscope is reflected on the micromodel and the image is then captured with a video camera and transferred either directly to a computer for digitizing or saved on videotape for later viewing. The fluids are injected either at constant rate using syringe pumps, or at constant pressure from pressurized reservoirs. The injection pressure is captured with pressure transducers and recorded in the computer.

4. Experimental Results

4.1. TWO-PHASE FLOW

When distilled, de-ionized water is first allowed to imbibe very slowly into a completely dry micromodel filled with air, a layer of water flows ahead of the main front through the crevices and corners, similar to observations by Dong and Chatzis (1995) for flow of a wetting liquid in a capillary tube. The approximately rectangular cross-section of the flow channels in the micromodel allows water to displace air from the corners. In Figure 8, a sequence of images captures the growth of the water layer in the crevices, until the water front displaces air from the pore space. The presence of the water layer can first be observed in Figure 8(b), and is also confirmed by the succession of gas snap-off events in the narrow pore throats as shown in Figures 8(c)–(f), which leaves trapped gas in the pore space.

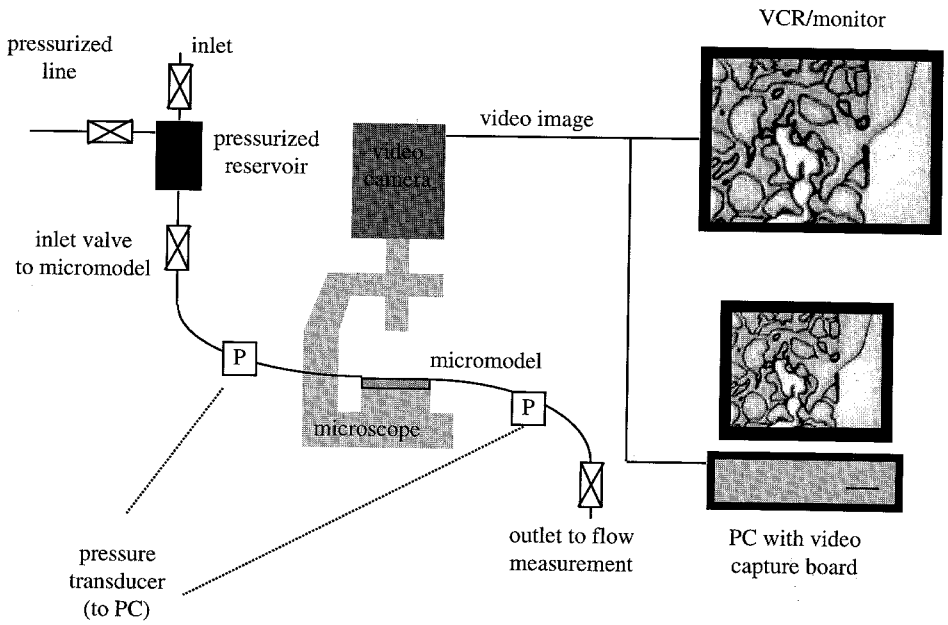

Figure 7. Experimental setup.

For drainage of the water saturated micromodel by air (Figure 9), the movement of the air front under even a small pressure drop across the micromodel of 10.4×10^3 Pa (1.5 psi) results in entrapment of water, due to by-passing. This corresponds to a pressure gradient of approximately 2×10^5 Pa m^{-1}, or around 10 Pa across a pore of length 50 μm. This compares with a capillary pressure of approximately 9.6×10^3 Pa in a pore of the same size. The wetting layer facilitates the flow of water out of these pockets (Figures 9(b)–(d)). However, as the layer of water thins, flow out of large pockets of by-passed water can be extremely slow, on the order of weeks or more. Very small pore bodies will not drain out because capillary forces hold the wetting fluid in place at thin pore throats.

In two-phase flow, we have observed gas invading water and water invading gas, both by snap-off and by piston-like advance, as well as flow in wetting layers.

4.2. THREE-PHASE FLOW

4.2.1. *Equilibrium Spreading Coefficient*

For three-phase flow, we studied the water–decane–air system, where according to literature values, $\gamma_{go} = 23.5 \times 10^{-3}$ N/m and $\gamma_{ow} = 52.0 \times 10^{-3}$ N/m at 24.5°C (Johnson and Dettre, 1966), with $C_s^e = -3.9 \times 10^{-3}$ N/m at equilibrium (Hirasaki, 1993). To verify the literature values of interfacial tensions (IFT) we measured them using the Drop-Weight Method (Adamson, 1990). We used certified grade decane

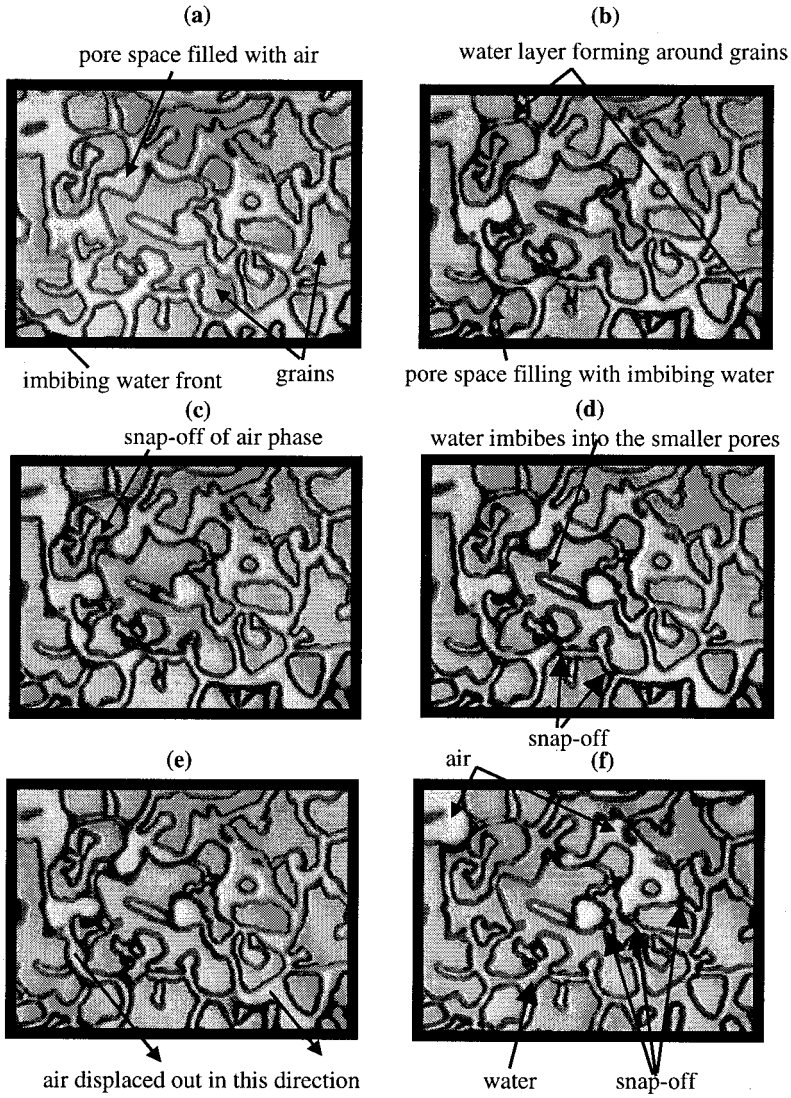

Figure 8. Imbibition of water into a dry micromodel: (a) the pore space is almost 100 per cent air saturated, with water imbibing from the lower left corner, (b) as water imbibes first into the crevices of the square corners through layers, it displaces the air towards the center of the pore space, (c) at the thinner pore throats, snap-off of the air phase occurs as the water layers on both sides join, (d) even before the gas phase is completely displaced, water imbibes into the thinner pores, flowing through the layers in the crevices, (e)–(f) at the end of the imbibition, many snap-off events occur in rapid succession, leaving some trapped air bubbles.

(Fischer, 99.8 per cent pure) and distilled and de-ionized water. We evaluated the IFT for pure fluids and for the three phases in contact for 24 h. The results are presented in Table I. The experimental $C_s^e = -4.1$ is very close to the literature

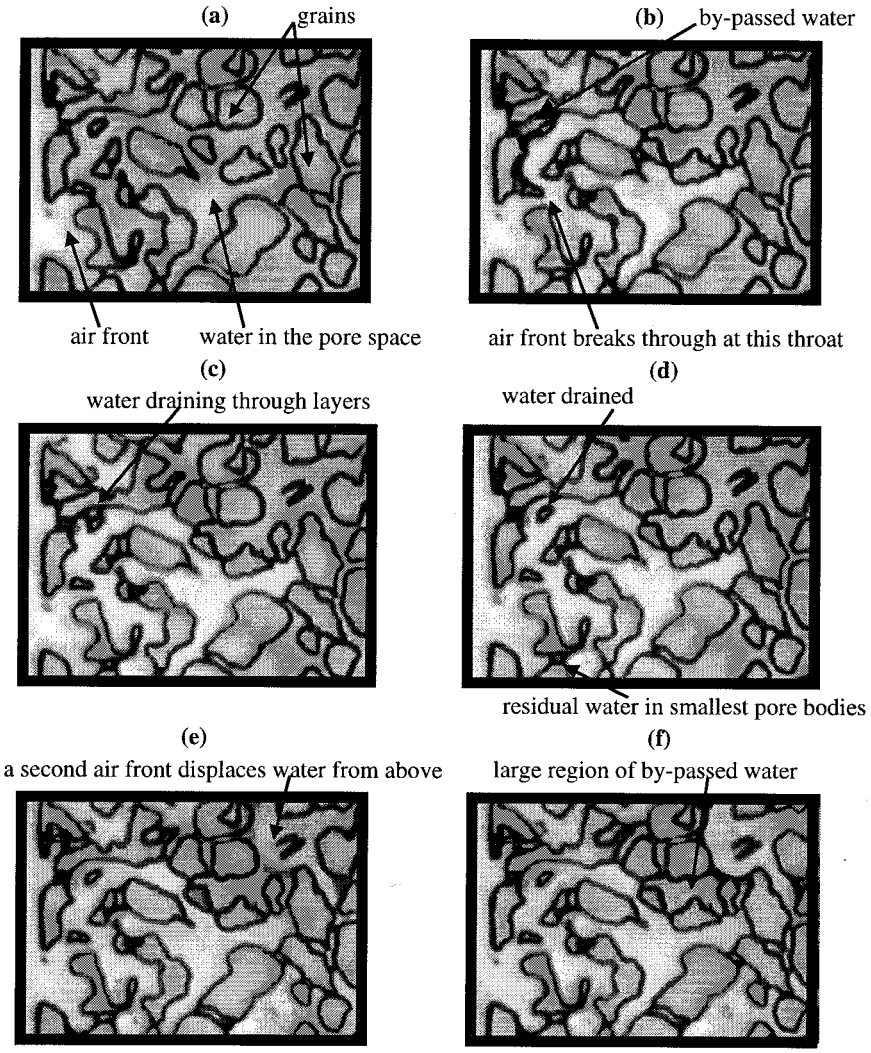

Figure 9. Water layers during air drainage of 100 per cent water saturated micromodel: (a) when the capillary entry pressure is exceeded, air enters the porous matrix, (b) as soon as the capillary pressure is exceeded for the next narrow pore throat, air quickly fills in the main pore bodies, by-passing water in the smaller pores, (c) water begins to drain from a small pore through the water layer, (d) drainage of the small pore is complete in only a few minutes, but water remains in smaller throats, (e) in an irregular pore space, the air front moves in less predictable modes, by-passing water either from above or below, (f) larger areas of by-passed water take a long time to drain, especially when the drainage is only through long, thin layers.

value. However, in a natural setting, all the IFTs would probably be lower, and further studies of IFTs of contaminated fluids are needed to determine experimental C_s^e for environmental conditions.

Table I. Experimental spreading coefficient

Interfacial tensions	Initial	In contact 24 h
Air–water, γ_{gw}	$71.6 \pm 0.2\,\mathrm{mN\,m^{-1}}$	$69.5 \pm 0.2\,\mathrm{mN\,m^{-1}}$
Air–decane, γ_{go}	$23.6 \pm 0.1\,\mathrm{mN\,m^{-1}}$	$23.4 \pm 0.1\,\mathrm{mN\,m^{-1}}$
Water–decane, γ_{ow}	$51.4 \pm 0.2\,\mathrm{mN\,m^{-1}}$	$50.2 \pm 0.2\,\mathrm{mN\,m^{-1}}$
Spreading coefficient, C_s^e	$-3.4 \pm 0.2\,\mathrm{mN\,m^{-1}}$	$-4.1 \pm 0.2\,\mathrm{mN\,m^{-1}}$

4.2.2. *Micromodel Observations*

The micromodel was first fully saturated with water. Then decane was introduced at a slow flow rate to displace water from the larger pore bodies. Only a small amount of decane was introduced, since we wanted to observe the displacement of oil at low saturation. As with air drainage, some water was by-passed as decane invaded the micromodel. Decane injection was stopped and then air was introduced at a very low pressure through the decane injection port.

The capillary entry pressure must be exceeded before air enters the micromodel. For air drainage of the water-wet micromodel, the capillary entry pressure into a pore much wider than it is deep, is given by

$$Pc_{gw} = \gamma_{gw} \cos\theta_{gw}/r, \tag{5}$$

with the radius, $r = 7.5\,\mu$m, determined by the etching depth of $15\,\mu$m, $\gamma_{gw} = 72 \times 10^{-3}$ N/m and $\cos\theta_{gw} = 1$, assuming a zero contact angle, resulting in a minimum injection pressure of 9.7×10^3 Pa (1.4 psi). However, when air enters through the decane port, the required capillary entry pressure is given by

$$Pc_{go} = \gamma_{go} \cos\theta_{go}/r. \tag{6}$$

The capillary entry pressure is then at most only 3.1×10^3 Pa (0.45 psi), since air displaces decane rather than water. The measured entry pressures are 10.4×10^3 Pa (1.5 psi) for air into a water-saturated model and 3.5×10^3 Pa (0.51 psi) for air through the decane port.

The volumetric flow rate, Q, was measured as 2.8×10^{-11} m^3/s (0.10 cm^3/h). Considering an average cross-sectional area, A, of 5×10^{-2} m by 15×10^{-6} m, and the definition for the capillary number

$$N_{\text{cap}} = \mu q/\gamma, \tag{7}$$

where μ is the viscosity of water, $q = Q/A$ and $\gamma = \gamma_{gw}$, then $N_{\text{cap}} \approx 5 \times 10^{-7}$. This flow rate was typical of most runs.

For stable oil layers in the water–decane–air system, Equation (2) constrains R to the range $0 < R < 0.26$, considering $\beta = 45^\circ$ for the square crevice in the micromodel and $\theta_{ow} = 0$. At $R_c = 0.26$, the theoretical ratio of capillary

pressures, Pc_{go}/Pc_{ow}, is 0.13. In our experiments, the pressure drop across the model is comparable with typical capillary pressures, which means that it is difficult to measure capillary pressures locally with any accuracy. However, the imposed pressure differences in the model implied $Pc_{go}/Pc_{ow} \approx 0.3$, and yet oil layers are still observed. Since the actual value θ_{ow} is greater than zero, R_c is in fact larger than 0.26. This analysis is thus consistent with the presence of oil layers in our experiments.

All the figures where three phases are present have been enhanced to clearly delineate the air (white), water (light gray) and decane (dark gray) phases, as well as the grains (medium gray), but the position and shape of the interfaces is as seen in the microscope. The sequence in Figure 10 presents the entry of air into the porous matrix, which contains decane and water. The air phase enters at a large pore throat. It is not initially apparent that air is surrounded by a layer of decane, but this becomes clear as the air phase first stops at the water/decane interface and the decane layer bulges out, displacing the surrounding water in the matrix (Figure 10(c)). This sequence demonstrates that oil layers of a non-spreading oil exist in the micromodel. Once the pore entry pressure is exceeded (Figure 10(d)), the air phase breaks into the rest of the porous matrix, displacing both decane and water. The sequence of images captures a DDI displacement (where air displaces water which displaces oil). This occurs since initially air contacts water directly before decane layers are formed. The water phase escapes through the crevices, and displaces oil at some other pore region not captured in these images. Due to the low injection pressures, the air front travels slowly into the matrix, as it must exceed the capillary pressure at each pore throat. The injection pressure is slowly increased to observe the displacements.

Double-drainage, where air displaces oil that displaces water, is observed in Figure 11. The advancing air phase is actually covered by a thin layer of decane, not apparent in the first images. As air advances under increasing injection pressure, it displaces decane (Figures 11(b) and (c)) which displaces water in the porous matrix. Snap-off of air within the decane layer occurs at pinched pore throats, resulting in disconnected air bubbles ahead of the main air front (Figure 11(d)).

The two images in Figure 12 present a double imbibition sequence. In this case, water is injected into the model containing decane and air. Air is continuous to the outlet and is surrounded by decane. Decane is being displaced by water. Figure 12(a) shows the air phase just before it is displaced. Water displaces decane that in turn displaces air. The whole process occurs in a fraction of a second. Double imbibition processes are extremely fast, especially when the initial water saturation in the matrix is very low. Although the overall process is double imbibition, in most of the micromodel the local displacements observed are two-phase imbibitions, and double imbibition is seldom observed.

IDI, where oil displaces water that displaces air, is captured in Figure 13. A large bubble of air is trapped, surrounded by water in the matrix. Decane is injected at an injection pressure of 41.6×10^3 Pa (6 psi). The decane front advances (Figure

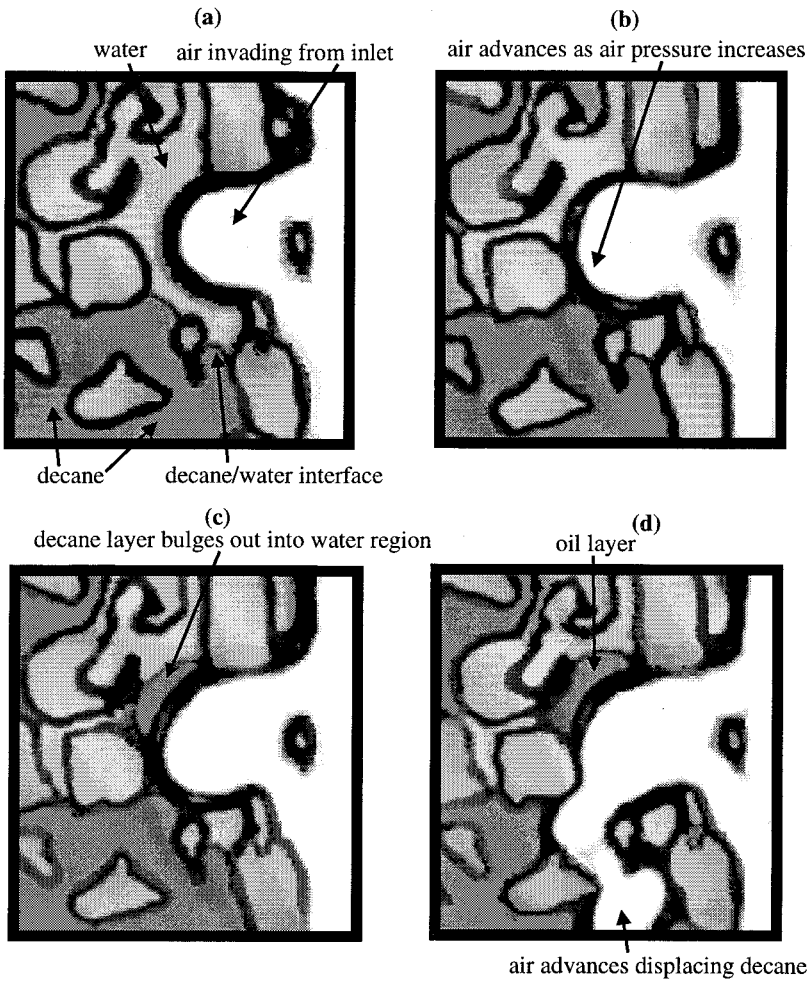

Figure 10. Water–decane–air system in the micromodel, showing oil layers: (a) air enters into the porous matrix which contains water and decane, (b) as the air pressure is slowly increased, the air front advances until it meets the water/decane interface, (c) the decane layer surrounding the air bubble bulges out into the water-saturated pore space, corroborating the existence of a decane layer, (d) once the decane–decane interface coalesces, the air front can move rapidly into the decane-filled pore space. A DDI displacement, air displacing water that displaces decane, is seen in Figure 10(b).

13(b)) displacing water but with little movement in the air/water interface. Figure 13(c) shows when the water becomes surrounded by decane and air, and water displacement must be through the crevices. Eventually, the pressure is sufficient to force decane to displace water that then displaces air (Figure 13(d)). In this sequence, there is direct contact of air by water, since decane has not yet contacted air. After decane contacts air, oil layers are observed and we do not see further IDI events.

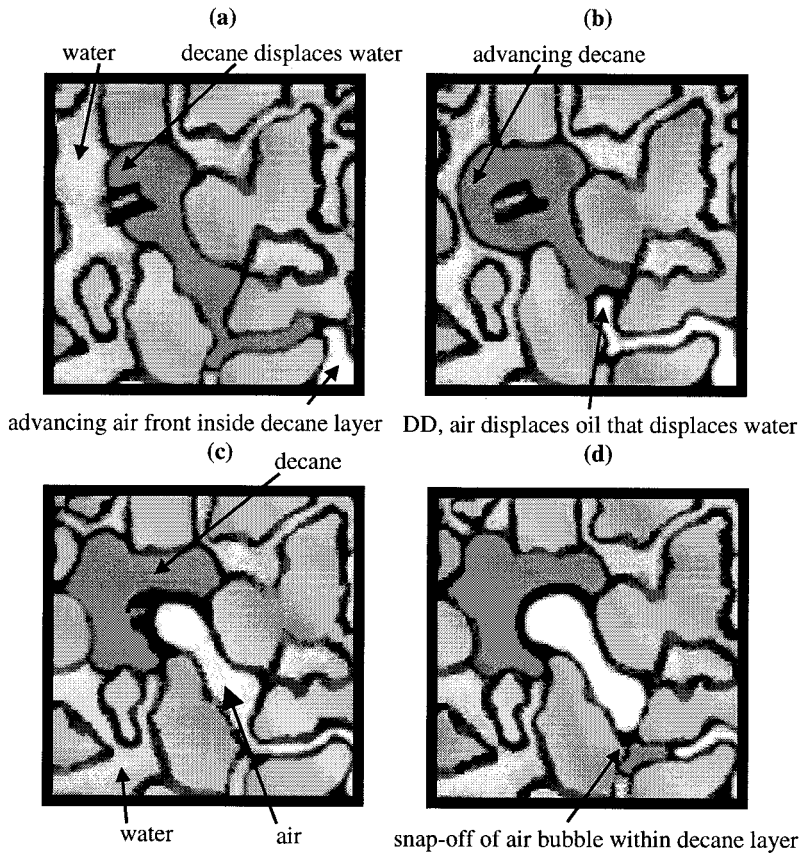

Figure 11. Double drainage sequence, with air displacing decane that displaces water, at the advancing water/decane interface: (a) air surrounded by decane, (b) as the air advances, decane is also forced into the surrounding water – this is double drainage, (c) air displaces decane, (d) snap-off of air front, leaving a disconnected bubble.

5. Discussion and Conclusions

Stable oil layers have been observed in a porous medium for the air–decane–water system which has a negative spreading coefficient. Four of the six possible double displacements have been observed, namely double drainage (DD), double imbibition (II), and drainage–imbibition with overall imbibition (IDI) and drainage–imbibition with overall drainage (DDI). Double drainage is the most commonly observed double displacement. Although double displacements occur, most of the displacements observed in a realistic pore space configuration involve only two phases in motion, with the third phase usually trapped by capillary forces. However, under three-phase conditions, water and oil layers play a significant role in drainage, by allowing both oil and water to flow at low saturation.

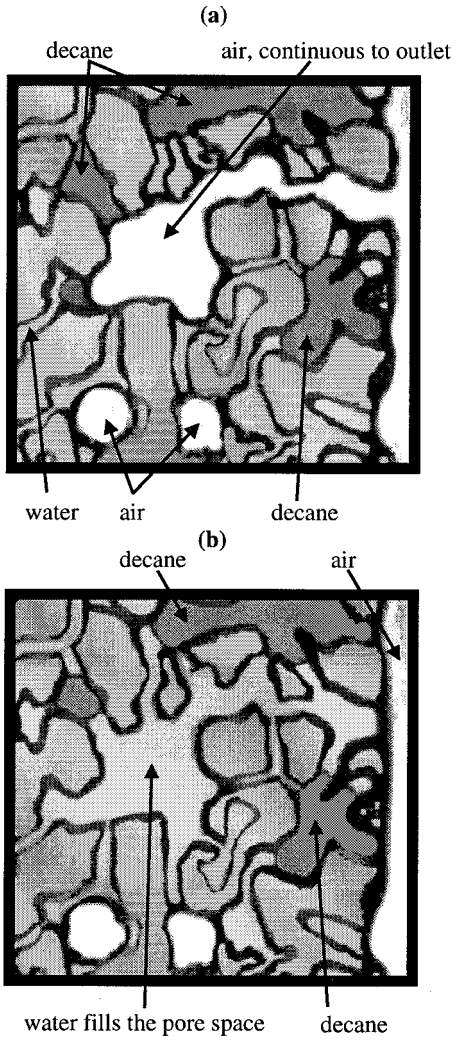

Figure 12. Double imbibition in the pore space: (a) air connected to the outlet port remaining after decane imbibition has either displaced most of the air or left it as trapped air bubbles. Water imbibition has also displaced most of the decane in the rest of the micromodel. (b) In one frame, water jumps across the pore space, displacing decane that displaces air.

In the presence of decane, direct gas/water displacements are not observed, except near the inlet, since a layer of oil surrounds the gas, which then does not contact the water directly. This explains why double drainage and double imbibition are readily observed, but the corresponding two-phase displacements do not occur, since gas and water do not directly contact each other. These observations are consistent with the work of Oren and Pinczewski (1992) and Soll *et al.* (1993). Moreover, the presence of oil layers between gas and water is the reason why the

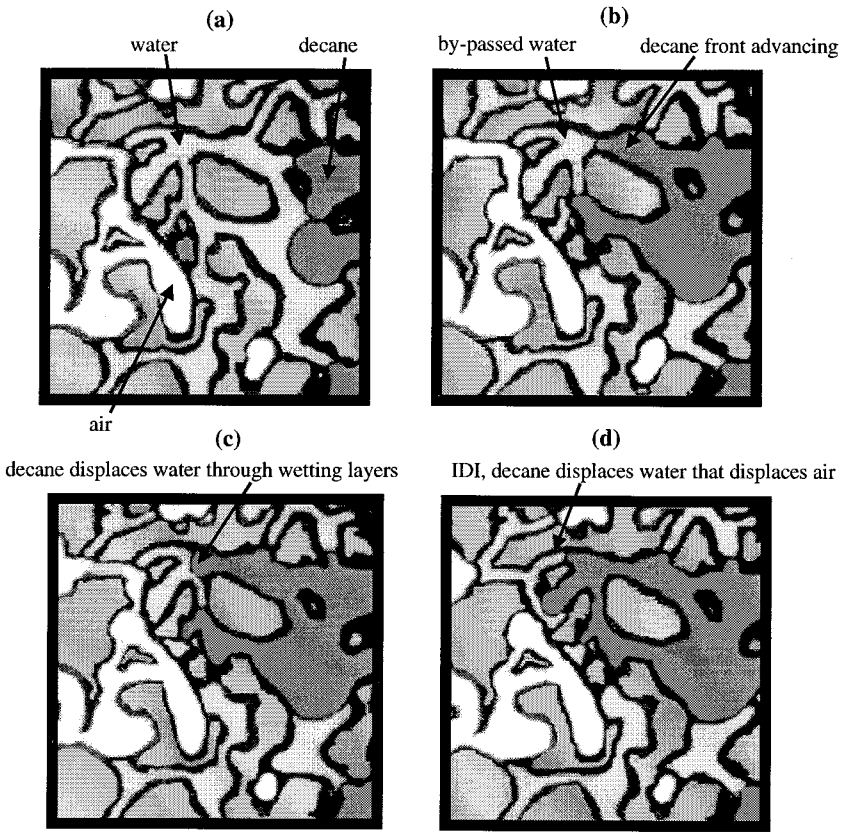

Figure 13. An IDI displacement, where oil displaces water that displaces air: (a) air is receding due to water imbibition, which is been displaced by decane, (b) decane completely surrounds water, which must now flow out either through the crevices or by displacing air, (c) water flows out through wetting layers, (d) finally decane displaces water that displaces air, flowing out through the top of the image, in an IDI displacement.

other double processes are much rarer, since they all involve a gas/water displacement as an intermediate step. In the IDI and DDI events we observed there were direct gas/water contacts, because gas had yet to contact decane.

During water drainage, wetting layers allow the outflow of the water, even for by-passed pockets of water. Thus, wetting layers result in a finite relative permeability of the wetting phase even at low wetting phase saturations.

The observed displacement mechanisms and the existence of water and oil layers can be used as input into a pore level numerical network model that can compute three-phase relative permeabilities and capillary pressures as a function of saturation, in a three-dimensional system (Fenwick and Blunt, 1996). From this, a physically based characterization of three-phase flow should be possible.

Acknowledgements

This research was partially funded by Project SU-95-4 from the Environmental Protection Agency and the Department of Defense through the Western Region Hazardous Substance Research Center, and Grant DACA39-95-K-0075 from the Department of Defense. The authors wish to thank Dr. Louis Castanier for insights on the construction and operation of the micromodels, as well as for the Scanning Electron Micrograph of the micromodel surface.

References

Adamson, A. W.: 1990, *Physical Chemistry of Surfaces*, 5th edn, John Wiley and Sons, New York.

Baker, L. E.: 1988, Three-phase relative permeability correlations, *Proceedings of the SPE/DOE Enhanced Oil Recovery Symposium*, Tulsa, Oklahoma.

Berkowitz, B. and Balberg, I.: 1993, Percolation theory and its application to groundwater hydrology, *Water Resour. Res.* **29** (4), 775–794.

Billiotte, J. A., De Moegen, H. and Oren, P. E.: 1993, Experimental micromodeling and numerical simulation of gas/water injection/withdrawal cycles as applied to underground gas storage, *SPE Advanced Tech. Series 1*, **1**, 133–139.

Blunt, M. J., Zhou D. and Fenwick, D. H.: 1995, Three phase flow and gravity drainage in porous media, *Transport in Porous Media* **20**, 77–103.

Blunt, M. J., King, M. J. and Scher, H.: 1992, Simulation and theory of two phase flow in porous media, *Phys. Rev. A* **46** (12), 7680–7699.

Blunt, M. J. and King, M. J.: 1991, Relative permeabilities from two- and three-dimensional pore-scale network modeling, *Transport in Porous Media* **6** (12), 407–433.

Chatzis, I., Kantzas, A. and Dullien, F. A. L.: 1988, On the investigation of gravity-assisted inert gas injection using micromodels, long Berea sandstone cores and computer-assisted tomography, SPE 18284, in *Proceedings of the 63rd Annual Technical Conference and Exhibition of the SPE*, Society of Petroleum Engineers, Houston, Texas, Oct. 2–5, 1988.

Dias, M. M. and Payatakes, A. C.: 1986, Network models for two phase flow in porous media. Part 1: Immiscible microdisplacements of non-wetting fluids, *J. Fluid Mech*. **164**, 305–336.

Dong, M., F., Dullien, A. L. and Chatzis, I.: 1995, Imbibition of oil in film form over water present in edges of capillaries with an angular cross section, *J. Colloid Interface Sci*. **172**, 21–36.

Dong, M. and Chatzis, I.: 1995, The imbibition and flow of a wetting liquid along corners of a square capillary tube, *J. Colloid Interface Sci*. **172**, 278–288.

Fayers, F. J.: 1989, Extension of Stone's method 1 and conditions for real characteristics in three phase flow, *SPE Reserv. Engng.* **4**, 437–445.

Fenwick, D. H. and Blunt, M. J.: 1996, Three dimensional modeling of three phase imbibition and drainage, *Adv. in Water Resour.* (in press).

Fenwick, D. H. and Blunt, M. J.: 1995, Pore level modeling of three phase flow in porous media, *8th European Symposium on Improved Oil Recovery*, Vienna, May 1995.

Ferrand, L. A. and Celia, M. A.: 1992, The effect of heterogeneity on the drainage capillary pressure-saturation relation, *Water Resour. Res.* **28** (3), 859–870.

Hirasaki, G. J.: 1993, Structural interactions in the wetting and spreading of van der Waals fluids, *J. Adhesion Sci. Technol.* **7** (3), 285–322.

Hornbrook, J.W., Castanier, L.M. and Pettit, P.A.: 1991, Observation of Foam/Oil interactions in a new high resolution micromodel, SPE 22631, Proceedings of the 66th Annual Technical Conference and Exhibition of the Society of Petroleum Engineers, Dallas, Texas, USA.

Jerauld, G. R. and Salter, S. J.: 1990, Effect of pore-structure on hysteresis in relative permeability and capillary pressure: pore-level modeling, *Transport in Porous Media* **5**, 103.

Johnson, R. E. and Dettre, R. H.: 1966, *J. Colloid Interface Sci*. **21**, 610–622.

Kalaydjian, F. J. M.: 1992, Performance and analysis of three phase capillary pressure curves for drainage and imbibition in porous media, SPE 24878, presented at the *67th Annual Technical Conference and Exhibition of the SPE*, Washington D.C.

Lenormand, R. and Zarcone, C.: 1988, Physics of blob displacement in a two-dimensional porous medium, *SPE Form. Eval.* 271–275.

Lenormand, R. and Zarcone, C.: 1983, Mechanisms of the displacement of one fluid by another in a network of capillary ducts, *J. Fluid Mech.* **135**, 337–353.

McDougall, S. R. and Sorbie, K. S.: 1995, The impact of wettability on waterflooding: pore-scale simulation, *SPE Reserv. Engng.* **10**, 208–213.

Mohanty, K. K., Gupta, A. and DeRuiter, R. A.: 1994, Pore-level mechanisms of residual oil formation during miscible displacement, *J. Colloid Interface Sci.* **163**, 199–216.

Oren, P. E. and Pinczewski, W. V.: 1995, Fluid distribution and pore-scale displacement mechanisms in drainage dominated three phase flow, *Transport in Porous Media* **20**, 105–133.

Oren, P. E. and Pinczewski, W. V.: 1992, The effect of wettability and spreading coefficients on the recovery of waterflood residual oil by miscible gas flooding, SPE 24881, *Proceedings of the 67th Annual Technical Conference and Exhibition of the SPE*, Washington, D.C.

Oren, P. E. and Pinczewski, W. V.: 1991, The effect of film flow on the mobilization of waterflood residual oil by immiscible gas flooding, *Proceedings of the 6th European IOR symposium*, Stavanger, Norway.

Oren, P. E., Billiote, J. and Pinczewski, W. V.: 1994, Pore-scale network modeling of residual oil recovery by immiscible gas flooding, SPE/DOE 27814, presented at the *9th Symposium on EOR*, Tulsa, OK, April 17–20, 1994.

Oren, P. E., Billiote, J. and Pinczewski, W. V.: 1992, Mobilization of waterflood residual oil by gas injection for water-wet conditions, *SPE Form. Eval.* **7** (1), 70–78.

Parker, J. C. and Lenhard, R. J.: 1990, Determining three-phase permeability-saturation-pressure relations from two phase system measurements, *J. Petrol. Sci. Eng.* **4**, 57–65.

Ransohoff, T. C. and Radke, C. J.: 1988, Laminar flow of a wetting liquid along the corners of a predominantly gas-occupied noncircular pore, *J. Colloid Interface Sci.* **121**, 392–401.

Sahimi, M.: 1993, Flow phenomena in rocks: from continuum models to fractals, percolation, cellular automata, and simulated annealing, *Rev. Mod. Phys.* **65**, 1393–1534.

Soll, W. E., Celia, M. A. and Wilson, J. L.: 1993, Micromodel studies of three-fluid porous media systems: pore-scale processes relating to capillary pressure-saturation relationships, *Water Resour. Res.* **29**:9, 2963–2974.

Soll, W. E. and Celia, M. A.: 1993, A modified percolation approach to simulating three-fluid capillary pressure-saturation relationships, *Adv. Water Resour.* **16**, 107–126.

Stone, H. L.: 1973, Estimation of three-phase relative permeability and residual oil data, *J. Can. Petrol. Tech.* **22**, 214–218.

Stone, H. L.: 1970, Probability model for estimating three-phase relative permeability, *J. Petrol. Tech.* **24** (4) 53–61.

Touboul, E., Lenormand, R. and Zarcone, C.: 1987, Immiscible displacements in porous media: testing network simulators by micromodel experiments, SPE 16954, presented at *62nd Annual Technical Conference and Exhibition SPE*, Dallas TX, Sept. 27–30, 1987.

van Genuchten, M. T.: 1980, A closed-form equation predicting the hydraulic conductivity of unsaturated soils, *Soil Sci. Soc. Amer. J.* **44**, 892–898.

Vizika, O., Avraam, D. G. and Payatakes, A. C.: 1994, On the role of the viscosity ratio during low-capillary-number forced imbibition in porous media, *J. Colloid Interface Sci.* **165**, 386–401.